Science of the Total Environment 664 (2019) 161–174

Contents lists available at ScienceDirect

Science of the Total Environment

journal homepage: www.elsevier.com/locate/scitotenv

Influences of 1.5 °C and 2.0 °C global warming scenarios on water use efficiency dynamics in the sandy areas of northern China☆

Xiaofei Ma [a,c], Chengyi Zhao [b,*], Wei Yan [d], Xiaoning Zhao [a]

[a] State Key Laboratory of Desert and Oasis Ecology, Xinjiang Institute of Ecology and Geography, Chinese Academy of Sciences, Urumqi 830011, China
[b] Land Science Research Center, Nanjing University of Information Science & Technology, Nanjing 210044, China
[c] University of Chinese Academy of Sciences, Beijing 100049, China
[d] School of Geographic Sciences, Xinyang Normal University, Xinyang 46400, China

HIGHLIGHTS

- The degree of WUE in different sandy land types under global warming of 1.5 °C and 2.0 °C was quantified.
- The prospective degree of desertification in northern China was estimated.
- Precipitation is not the dominant factor of WUE change in sandy area in northern China.
- WUEs of different sandy land types were mainly influenced by meteorological and vegetation factors.
- Desertification degree comprehensively reflects the linkage between the SPEI, LAI and WUE.

GRAPHICAL ABSTRACT

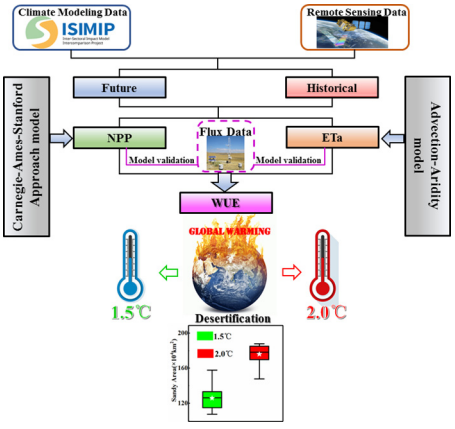

ARTICLE INFO

Article history:
Received 28 September 2018
Received in revised form 29 January 2019
Accepted 30 January 2019
Available online 31 January 2019

Editor: James Cleverly

Keywords:
WUE
1.5 °C warming
2.0 °C warming
Desertification
Northern China

ABSTRACT

Water use efficiency (WUE) is an important variable used in hydrometeorology study to reveal the links between carbon-water cycles in sandy ecosystems which are highly sensitive to climate change and can readily reflect the effects of it. In light of the Paris Agreement, it is essential to identify the regional impacts of 0.5 °C of additional global warming to inform climate adaptation and mitigation strategies. Using the modified Carnegie-Ames-Stanford Approach (CASA) and Advection-Aridity (AA) models with global warming values of 1.5 °C and 2.0 °C above preindustrial levels from Inter-Sectoral Impact Model Intercomparison Project (ISIMIP2b) datasets, we conducted a new set of climate simulations to assess the effects of climate on WUE (the ratio of net primary productivity (NPP) to actual evapotranspiration (*ETa*)) in different sandy land types (mobile sandy land, MSL; semimobile/semifixed sandy land, SMSF; and fixed sandy land, FSL) during the period of baseline (1986–2005) and future (2006–2100). The spatiotemporal patterns of *ETa*, NPP, and WUE mostly showed increasing trends; the value of WUE decreased (6.40%) only in MSL with an additional 0.5 °C of warming. Meteorological and vegetation factors determined the variations in WUE. With warming, only the correlation between precipitation and WUE decreased in the three sandy land types, and the leaf area index (LAI) increased with an additional 0.5 °C of warming. The desertification degree comprehensively reflects the linkages among the standardized precipitation

☆ Funding information: National Natural Science Foundation of China, Grant/Award Numbers: 41671030, U1403281. The Natural Science Foundation of Jiangsu Province, Grant/Award Number: BK20181059. The National Basic Research Program of China, Grant/Award Number: 2013CB429903. Thousand Young Talents Program, Chinese Academy of Sciences, Grant/Award Number: Y772121.

* Corresponding author.
E-mail address: zhaocy@nuist.edu.cn (C. Zhao).

https://doi.org/10.1016/j.scitotenv.2019.01.402

evapotranspiration index (SPEI), LAI and WUE. Simulation results indicated the sandy area extent could potential increase by 20×10^4 km^2 per decade on average during 2016–2047 and that the increase could be gradual (2.60×10^4 km^2 per decade) after 2050 (2050–2100). These results highlight the benefits of limiting the global mean temperature change to 1.5 °C above preindustrial levels and can help identify the risk of desertification with an additional 0.5 °C of warming.

1. Introduction

Water plays an important role in plant growth; accordingly, it may also influence carbon assimilation through plant photosynthesis (Baldocchi, 1994; Yu et al., 2004). Determining how the availability of water influences carbon assimilation throughout an ecosystem is also important for evaluating the possible impacts of climate change (Jassal et al., 2009). Moreover, it is necessary to employ WUE (water use efficiency), a critical variable reflecting the coupled relation between the water and carbon cycles, in studies of hydrology and climate change (Yu et al., 2008). Generally, WUE is defined as the ratio between carbon gain and water loss, which are quantified as NPP (net primary productivity) and *ETa* (actual evapotranspiration), respectively, in this paper (Fischer and Turner, 1978; Jiao et al., 2018; Zhang et al., 2016; Zhao et al., 2004). It is similarly critical to examine the ecosystem WUE, which serves as a key indicator of carbon-water cycle coupling (Ito and Inatomi, 2012) and is fundamental both for understanding eco-hydrological processes and for promoting sustainable development (Lu and Zhuang, 2010; Tian et al., 2010; Zhang et al., 2016). Analyzing the driving factors and the characteristics of spatial and temporal variations in the WUE of an ecosystem can help clarify how terrestrial ecosystems respond and adapt to climate change worldwide (Gao et al., 2014; Liu et al., 2015; Tian et al., 2011).

Drought represents a major climate disturbance worldwide, and the frequency and intensity of droughts are expected to increase during this century (IPCC, 2013). Drought increases the ET rate of an ecosystem and reduces carbon sequestration, thereby affecting the carbon-water cycle across the Earth (Battipaglia et al., 2014; Gang et al., 2016; Yu et al., 2017). In particular, drought has become an important factor restricting the sustainable development of sandy areas throughout northern China, which span three bioclimatic zones: arid, semiarid and semihumid zones. Therefore, exploring the spatial and temporal variations in the WUE of these areas under future climate change scenarios can help us better understand the desertification occurring in these areas.

The existence of global warming has become indisputable (IPCC, 2013). Recently, the signatories of the Paris Agreement aspired to control the average global temperature rise to within 2.0 °C above the preindustrial level, with controls within 1.5 °C above the preindustrial level to be achieved through best efforts (Frieler et al., 2017). This commitment was expected to remarkably reduce the risks and influences of climate change (Fawcett et al., 2015). However, no complete assessment of the regional influences of these worldwide climate policy targets has been performed. Moreover, the effect of desertification resulting from global warming on the expansion of sandy areas remains uncertain (Ma et al., 2018). According to their features, sandy areas can generally be categorized into mobile, semimobile/semifixed and fixed sandy land (MSL, SMSF, and FSL, respectively) (Duan et al., 2001; Hao and Wu, 2006; Li et al., 2007; Zhou et al., 2013). These different categories of sandy land collectively account for 28% of the total land area in China (Zhang and Huisingh, 2018), and the sandy areas of northern China comprise the core area of the Silk Road Economic Belt. Of the many influences limiting the economic development of this region, environmental problems, such as sparse vegetation, drought and water scarcity, have become the dominant factors.

WUE is critical for regulating water resources and ensuring the stability of sand-fixing vegetation in sandy areas. Liu et al. (2015) evaluated the WUE of terrestrial ecosystems in China using ecosystem process models and in situ observation data and noted regional differences in the effects of drought on WUE. Zhu et al. (2015) showed that the WUE decreased with increasing latitude in China. At the regional scale, Zhang et al. (2016) estimated the WUE of the Loess Plateau in China from 2000 to 2010 using MODIS (Moderate Resolution Imaging Spectroradiometer) ET products and the CASA (Carnegie-Ames-Stanford Approach) model. Based on long-term observation data, Keenan et al. (2013), Huang et al. (2015), and Sun et al. (2016) noted that increases in the CO_2 concentration, precipitation and temperature each have different effects on WUE. However, although data on the carbon-water budget of monitoring stations can be captured accurately, the scale of such research is often small. In addition, the application of MODIS products to sandy land poses a challenge because MODIS performs poorly (*ETa* and NPP) in these areas (Tao et al., 2017). Based on the above considerations, the present study used data from the ISIMIP2b (Inter-Sectoral Impact Model Intercomparison Project) climate model in conjunction with the CASA and AA (Advection-Aridity) models to estimate the future NPP and *ETa*, respectively; then the changes in the WUE of sandy areas throughout northern part China under two global warming scenarios were explored.

Consequently, our objectives are (1) to understand the temporal and spatial variations in the WUE of different sandy areas throughout northern China under global warming scenarios of 1.5 °C and 2.0 °C; (2) to analyze the impacts of climatic factors on WUE under global warming scenarios of 1.5 °C and 2.0 °C; and (3) to construct the relationship between WUE and the process of desertification and to analyze the future degree of desertification in the sandy areas of northern China. This research provides a basis for further interpretation of climate change characteristics and future emission reduction studies in sandy areas under different global warming conditions. These results can help identify the risk of desertification with an additional 0.5 °C of warming.

2. Materials and methods

2.1. Study area

The sandy areas in the northern region of China, which is distributed across 35°–50° N, 75°–125° E, extend from the western Tarim Basin to the eastern edge of the Songnen Plain, forming an arcuate-shaped desert belt that crosses the semihumid, semiarid and arid climate zones in the northwestern region of China (Du et al., 2018; Li et al., 2004b). This desert area covers 4500 km in the east-west direction and 600 km in the south-north direction (Li et al., 2004a; Ma et al., 2018; Zhang et al., 2018), occupying 28% of the total land area of China and spanning four climatic zones: semihumid, semiarid, arid and extremely arid areas. Generally, the annual precipitation ranges from 30 mm (in the western part) to 450 mm (in the eastern part).

When classified according to the differences in their dune mobility and climate, the sandy lands in China can be further divided into a western desert region and an eastern desert region with the Helan Mountains as the boundary (Dong et al., 2016; Li et al., 2017; Zhang et al., 2018). Generally, the sandy areas in the northern region of China are formed by a plurality of entities, including (from west to east) the Qinghai Gonghe Sandy Land, Gurbantunggut Desert, Taklimakan Desert, Qaidam Desert, Kumtag Desert, Badain Jaran Desert, Tengger Desert, Ulanbuh Desert, Hobq Desert, Mu Us Sandy Land (in addition to the adjacent pastoral and agricultural zones to the north), Otindag Sandy

Land, Horqin Sandy Land and Hulunbuir Sandy Land. Moreover, a wilderness transition zone and a desert are also included in northern China. The environment in this zone has been seriously affected by climate change and destructive human activities; as a result, this region is highly sensitive and vulnerable (Wang et al., 2012; Wang and Dickinson, 2012). According to monitoring data, the area of desertification in China increased by 4.6×10^4 km^2 from 1988 to 2000 and decreased by 1.5×10^4 km^2 from 2000 to 2015 (Q.F. Liu et al., 2018; Zhang and Huisingh, 2018). Despite the reverse trend of desertification in China over the last fifteen years, the area of desertification has still increased with a net growth of 8.6×10^4 km^2 since the early 1950s, which is equivalent to the area of two Tengger Deserts (Li et al., 2004a; Li et al., 2004b; Wang et al., 2013). Two terms were defined in this study. The first term is desert, defined as the transition area from semiarid land to arid land that is less covered by vegetation but is dominated by MSL. The second term is sandy land, defined as the transition area from semihumid land to semiarid land that is covered by little or moderate vegetation and is dominated by SMSF and FSL (Fig. 1).

To validate the results of the data simulation, records of meteorological observations and flux data were collected from five representative sand flux sites, as shown in Fig. 1, which belong to CERN (China Ecosystem Research Network, http://www.cern.ac.cn) and ChinaFLUX (Chinese FLUX Observation and Research Network, http://www.Chinaflux.org). These five sites located in different types of sandy land and in different bioclimatic zones are capable of accurately reflecting the WUE in the sandy areas of northern China (Yu et al., 2006) (Table 1).

2.2. Data

2.2.1. Vegetation data

The LAI (leaf area index) dataset for the period of 1982–2015 was obtained from fifteen-day NDVI (normalized difference vegetation index) composite data based on the NDVI-LAI table (Xiao et al., 2014). The standing NDVI dataset was developed from the AVHRR (Advanced Very High-Resolution Radiometer) sensors on board the NOAA (National Oceanic and Atmospheric Administration) series of satellites (ftp://ftp.glcf.umd.edu). This study evaluated the LAI by using products from GLASS (Global Land Surface Satellite) (http://glass-product.bnu.edu.cn). The GLASS products, which have a spatial resolution of 0.05°, were based on the optimized processing of MODIS data. Historical GLASS and AVHRR NDVI products boast a wide range of applications in monitoring the variations in land surface properties such as vegetation activity (Pettorelli et al., 2005; Xiao et al., 2014). Furthermore, future vegetation datasets (2016–2100) were obtained from http://data.ess.tsinghua.edu.cn; these datasets have been used mainly to evaluate the global land cover under different emission scenarios in future periods, and they have been applied in many fields. From these data, we computed the future (2016–2100) NDVI and land use. In addition, 1:100,000 scale vegetation type maps of China were used to collect vegetation type data; the statistics of these maps originated from the Resources and Environment Science Data Center of the Chinese Academy of Sciences of China (http://www.resdc.cn). The main vegetation type codes served as benchmarks during the processing and merging procedures in this study (Zhang and Zhang, 2017). In this paper, the NDVI SR (simple ratio) in the CASA model was evaluated by the acquired NDVI data (1986–2100), and the characteristics of future LAI changes were evaluated by establishing the relationship between the LAI data and WUE.

2.2.2. Land cover data

The MODIS instrument is an important sensor installed on the Terra satellite and the Aqua satellite, both of which are a part of the EOS (Earth Observing System) operated by NASA (National Aeronautics and Space Administration), an independent agency of the United States. Having been sufficiently validated, MODIS data products are extensively used globally (Friedl et al., 2010; Hu and Jia, 2015; Mu et al., 2011b). This paper adopted the annual MCD12Q1 land cover type product (resolution of 500 m) (http://landsweb.nascom.nasa.gov) on the basis of the classification by the IGBP (International Geosphere-Biosphere Programme) (Loveland and Belward, 1997). In this study, the historical

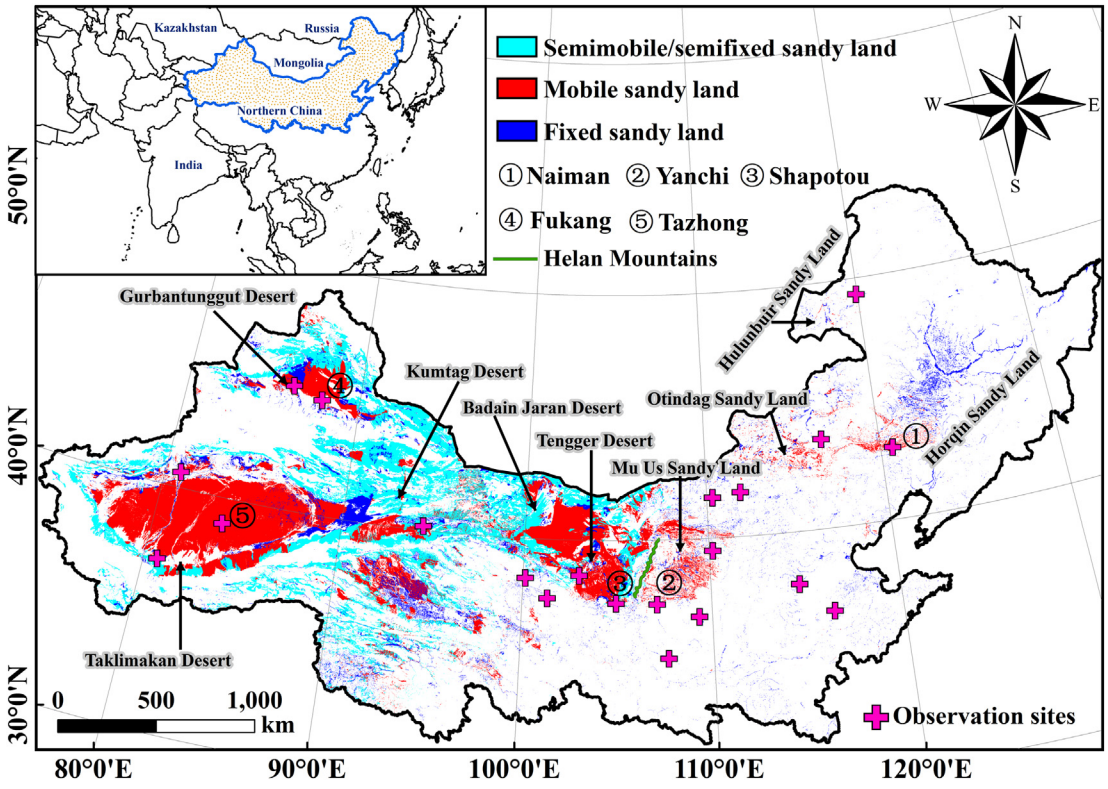

Fig. 1. Locations of the sandy areas in northern China.

Table 1
Information on the five flux sites in the sandy areas of northern China.

Site name	Lat (°N)	Lon (°E)	Precipitation (mm)	Elevation (m)	Bioclimatic region	Sand type	References
Naiman	42.93	120.7	366.4	361	Semihumid	FSL	Zheng et al. (2017)
Yanchi	37.4	107.12	295	442	Semiarid	SMSF	Fu et al. (2006)
Shapotou	37.53	105.8	186.6	1227	Arid	SMSF	Zheng et al. (2017)
Fukang	42.28	87.92	160	482	Arid	SMSF	Yu et al. (2006)
Tazhong	38.97	83.65	22.8	1082	Extremely arid	MSL	Yang et al. (2013)

Note: MSL, mobile sandy land; SMSF, semimobile/semifixed sandy land; FSL, fixed sandy land.

(1986–2015) land use data for the sandy areas of northern China were computed from the MCD12Q1 product data. These historical data were then used to evaluate ε_{max} in the CASA model and to calculate the area of desertification in northern China over the historical period.

2.2.3. Climate modeling data

This study employed four models from ISIMIP2b (https://www.isimip.org), namely, the MIROC5 (Model for Interdisciplinary Research On Climate) model, the IPSL-CM5A-LR (Institut Pierre-Simon Laplace Climate Model 5A-Low Resolution) model, the HadGEM2-ES (Hadley Centre Global Environmental Model version 2 Earth System configuration) model and the GFDL-ESM2M (Geophysical Fluid Dynamics Laboratory Earth System Modular Ocean Model) model, as shown in Table 2, and all of the data were projected by GCMs (general circulation models). From these models, daily output data, such as the specific humidity, relative humidity, snowfall flux, precipitation, shortwave and longwave radiation, wind speed, atmospheric pressure and air temperature (minimum and maximum), can be obtained. The reference period of 1986–2005 was used to assess the historical WUE value and determine the ISIMIP2b data. Moreover, the expected WUE variations under different RCPs (representative concentration pathways) during the period of 2006–2100 were analyzed. To facilitate a comparison, the datasets of these four models were gridded for the northern region of China for a second time with a bilinear interpolation algorithm until the horizontal grid resolution reached 0.5° × 0.5°. In addition, we used MME (multimodel ensemble) technology to evaluate the WUE.

The global warming scenarios of 1.5 °C and 2.0 °C can be defined using different methods (King et al., 2017). In addition, due to the differences among the datasets employed for this purpose, the evaluation results diverge (the 1.5 °C and 2.0 °C warming thresholds are reached at different points in time). For instance, according to the ISIMIP data, the 1.5 °C and 2.0 °C warming thresholds will be reached in 2020–2039 (RCP2.6, which corresponds to radiative forcing increase of 2.6 W/m^2 in the year 2100 relative to preindustrial values) and 2040–2059 (RCP4.5) (Warszawski et al., 2014). Therefore, the occurrence times of the 1.5 °C and 2.0 °C warming thresholds were used to estimate the WUE in the sandy areas in our study region.

2.3. Methods

2.3.1. AA model for estimating ETa

Although the AA model (Brutsaert and Stricker, 1979) based on complementarity uses a relatively small number of parameters and a simple algorithm, its accuracy is extremely high (Su et al., 2017). Thus, this model has been widely applied to the calculation of *ETa* in recent years (Haque, 2003; Li et al., 2013a). The equations of the AA model are as follows:

$$ET_p = \frac{\Delta(R_n - G)}{\Delta + \gamma} + \frac{\Delta E_a}{\Delta + \gamma} \tag{1}$$

$$ET_c = \alpha \frac{\Delta(R_n - G)}{\Delta + \gamma} \tag{2}$$

$$\gamma = \frac{C_P P}{\varepsilon \lambda} \tag{3}$$

$$\Delta = \frac{4098 e_a^*}{(T + 237.3)^2} \tag{4}$$

$$E_a = f(u)(e_a^* - e_a) \tag{5}$$

$$\mathrm{ET}_a = 2ET_c - ET_p \tag{6}$$

Eqs. (1)–(6) can be used to obtain the *ETa* distribution:

$$ET_a = (2\alpha - 1)\frac{\Delta}{\Delta + \gamma}(R_n - G) - \frac{\Delta}{\Delta + \gamma}E_a \tag{7}$$

where ET_c is the wet environment ET, ET_p denotes potential evapotranspiration, C_P refers to the specific heat of air under ordinary atmospheric conditions, γ refers to the constant value of the humidity in the calculation, P refers to the barometric pressure, λ refers to the latent heat of evaporation, ε refers to the molecular water-air weight ratio, Δ refers to the curve of the saturated vapor pressure at the ambient temperature, R_n refers to the net radiation close to the surface that manifests in terms of an equivalent vaporization rate, e_a^* and e_a represent the saturated vapor pressure and the actual vapor pressure, respectively, G refers to the heat flux of soil, $f(u)$ is a function of the wind speed u, and α refers to the Priestley-Taylor evaporation coefficient, which varies in space relative to the features of underlying surfaces. The values of α, which fall within the range of 0.913–0.997, were extracted from the studies by Li et al. (2004a) and Jian et al. (2018), and these values were employed for the four bioclimatic zones in which the sandy areas of northern China are located.

2.3.2. CASA model for estimating NPP

The CASA model is a light use efficiency-related model based on remote sensing that assesses the NPP per pixel each month (Piao et al., 2005). The NPP calculated by this model is the product of the light use efficiency (ε, units: g C/MJ), through which the APAR (absorbed photosynthetically active radiation; unit: MJ/m^2) is converted into greater plant biomass, and the amount of PAR (photosynthetically active radiation) that green vegetation absorbs (i.e., APAR) (Liang et al., 2015). The CASA model equations are expressed as follows:

$$\mathrm{NPP}(x,t) = APAR(x,t) \times \varepsilon(x,t) \tag{8}$$

$$\mathrm{APAR}(x,t) = \mathrm{SOL}(x,t) \times \mathrm{FPAR}(x,t) \times 0.5 \tag{9}$$

$$\mathrm{FPAR}(x,t) = \frac{(SR(x,t) - SR_{min})}{(SR_{max} - SR_{min})} \times (FPAR_{max} - FPAR_{min}) + FPAR_{min} \tag{10}$$

Table 2
List of the ISIMIP2b models used in the analysis.

Model	Originating group	Resolution (Lon × Lat)
GFDL-ESM2M	Geophysical Fluid Dynamics Laboratory, United States	144 × 90
HadGEM2-ES	Met Office Hadley Center, United Kingdom	145 × 192
IPSL-CM5A-LR	Institut Pierre-Simon Laplace, France	96 × 96
MIROC5	Atmosphere and Ocean Research Institute, Japan	256 × 128

$$SR(x,t) = \frac{1 + NDVI(x,t)}{1 - NDVI(x,t)} \tag{11}$$

$$\varepsilon(x,t) = T_{\varepsilon 1}(x,t) \times T_{\varepsilon 2}(x,t) \times W_{\varepsilon}(x,t) \times \varepsilon_{max} \tag{12}$$

$$T_{\varepsilon 1}(x,t) = 0.8 + 0.2 \times T_{opt}(x) - 0.0005 \times \left[T_{opt}(x)\right]^2 \tag{13}$$

$$T_{\varepsilon 2}(x,t) = \frac{1.184}{\left\{1 + e^{\left[0.2 \times \left(T_{opt}(x) - 10 - T(x,t)\right)\right]}\right\}} \times \frac{1}{\left\{1 + e^{\left[0.3 \times \left(-T_{opt}(x) - 10 + T(x,t)\right)\right]}\right\}} \tag{14}$$

$$W_{\varepsilon}(x,t) = 0.5 + \frac{0.5 \times EET(x,t)}{PET(x,t)} \tag{15}$$

where t refers to time, x refers to a specific geographical coordinate, FPAR (fraction of photosynthetically active radiation), which is obtained from the NDVI data, refers to the PAR absorbed by the vegetation canopy, the coefficient 0.5 shown in Eq. (9) indicates that approximately half of all incident solar rays fall in the PAR waveband (0.4–0.7 μm) (Potter et al., 1993), and SOL refers to the total amount of solar radiation. Eq. (10) shows that FPAR can serve as a linear function for the calculation of the NDVI SR, the computation of which is performed with Eq. (11) (Field et al., 1995). ε_{max} refers to the largest light use efficiency, which was calculated in this study through the methods described in a previous domestic study (Zhu et al., 2006). However, Zhu et al. (2006) calculated ε_{max} by using GLC2000 land use classification data, which differ slightly from the MCD12Q1 land use data applied to the present study.

2.3.3. Computation of drought indices

In the context of global warming, the SPEI (standardized precipitation evapotranspiration index) has been broadly applied to monitor the severity of drought by meteorological communities (Tao et al., 2014; Yao et al., 2018). To describe how the evaporative demand changes, the SPEI combines the sensitivity of the PDSI (Palmer drought severity index) with that of the SPI (standardized precipitation index) (Vicente-Serrano et al., 2010; Wang et al., 2015). In this paper, we used the SPEI (Vicente-Serrano et al., 2010) to evaluate the variability of drought. The SPEI value is calculated using precipitation (P) and ET_p. The computation of the SPEI (Vicente-Serrano et al., 2010) includes three steps: (1) estimating the monthly ET_p using Eq. (1); (2) determining the accumulated water deficit D (=P-ET_p), which is normalized into a log-logistic probability distribution; and (3) obtaining the SPEI through Eqs. (15) and (16).

$$f(x) = \left[1 + \left(\frac{\alpha}{x - \gamma}\right)^{\beta}\right]^{-1} \tag{16}$$

$$\mathrm{SPEI} = W - \frac{c_0 + c_1 W + c_2 W^2}{1 + d_1 W + d_2 W^2 + d_3 W^3} \tag{17}$$

where $f(x)$ refers to the PDF (probability distribution function) of D, α refers to the scale of the Pearson III distribution, β refers to the shape of the Pearson III distribution, and γ refers to the original parameter of the Pearson III distribution (Singh et al., 1993; Vicente-Serrano et al., 2010). In the case that $P(D) \le 0.5$, $P(D) = 1 - f(x)$ and $W = \sqrt{-2 \ln P(D)}$; in the case that $(D) > 0.5$, P(D), (1- P(D))=1 − $f(x)$, where the sign of the SPEI is reversed.

2.3.4. WUE trend analysis

As shown in Eq. (18), the rate of dynamic change in the WUE in each pixel was simulated by using a linear regression approach (Stow et al., 2003), where n and WUE_i were used to represent the number of years and the WUE value in a specific year, respectively. The existence of a *slope* allows the assumption of an increased WUE value. The *CV* (coefficient of variation) is employed to measure the fluctuations in the WUE in each pixel corresponding to the specific year, as shown in Eq. (19), where the *CV* value forms a negative correlation with the WUE stability. σ is used to describe the SD (standard deviation) of the WUE value in each pixel; in this study, the average was applied. Herein, Eqs. (18) and (19) were programmed through IDL7.1 (Interactive Data Language version 7.1) so that large raster datasets can be processed in batches. The equations for the *slope* and *CV* are as follows:

$$\theta_{slope} = \frac{n \times \sum_{i=1}^{n}(i \times WUE_i) - \sum_{i=1}^{n} i \sum_{i=1}^{n} WUE_i}{n \times \sum_{i=1}^{n} i^2 - \left(\sum_{i=1}^{n} i\right)^2} \tag{18}$$

$$\mathrm{CV} = \frac{\sqrt{\frac{1}{n}\sum_{i=1}^{n}(x_i - \overline{x})^2}}{\frac{1}{n}\sum_{i=1}^{n} x_i} \tag{19}$$

To further illustrate the variation in the WUE, we calculated the value of R/F for each pixel. The correlation coefficient R was employed to calculate the goodness of fit of the two variables, and the F test was used to analyze the level of significance. The values of R and F were computed using the following equations:

$$\mathrm{R} = \frac{n \times \sum_{i=1}^{n}(i \times WUE_i) - \sum_{i=1}^{n} WUE_i \times \sum_{i=1}^{n} i}{\sqrt{n \times \sum_{i=1}^{n} i^2 - \left(\sum_{i=1}^{n} i\right)^2} \times \sqrt{n \times \sum_{i=1}^{n} WUE_i{}^2 - \left(\sum_{i=1}^{n} WUE_i\right)^2}} \tag{20}$$

$$\mathrm{F} = \frac{(n-2) \times \sum_{i=1}^{n}\left(\widehat{WUE_i} - \overline{WUE}\right)}{\sum_{i=1}^{n}\left(WUE_i - \widehat{WUE_i}\right)} \tag{21}$$

where R is the correlation coefficient, F is the value obtained from the F test, $\widehat{WUE_i}$ is the regressed WUE value in year i, and $\overline{WUE}$ is the average WUE value over the study period. The statistical p value of the F test can be classified as either significant ($p < 0.05$) or not significant ($p > 0.05$).

2.4. Model validation

Based on the field observation data (bar chart) from five flux observation stations, the WUE values were calculated and compared with the mean (scatter plot) of the 4 climate data simulation results (Fig. S1). The findings suggest that the observed values are consistent with the simulated values ($R^2 \ge 0.47$). Through the model adopted in this paper, it is feasible to evaluate the WUE in the sandy areas of northern China in accordance with the data of the four climate models considered herein.

3. Results

3.1. Spatial dynamics of WUE/NPP/ETa under global warming scenarios of 1.5 °C and 2.0 °C

Under the two global warming scenarios (1.5 °C and 2.0 °C), certain differences are observed in the spatial distributions of *ETa*, NPP and WUE in the sandy areas of northern China (Fig. 2). Under these scenarios, the spatial distribution of *ETa* decreases gradually from east to west. Under the two global warming scenarios (1.5 °C and 2.0 °C), the maximum values of *ETa* (48.72 mm and 77.54 mm, respectively) appear in the southeastern part of the study region. In comparison with the reference period of 1986–2005, the regions with negative *ETa* growth are located mainly in the northwestern part of the study region under

the 1.5 °C warming scenario (Fig. 2. a). The minimum *ETa* value is −8.47 mm, and low values, which are distributed mainly in the Taklimakan and Badain Jaran Deserts, account for 27.60% of the total study area. Correspondingly, under the warming scenario of 2.0 °C (Fig. 2. b), the *ETa* distribution is spatially banded. During the same reference period ($P < 0.01$), the area exhibiting negative *ETa* growth decreased significantly by 7.58%.

The spatial distributions of NPP differ largely between these two temperatures rise scenarios. Under the warming scenario of 1.5 °C (Fig. 2. c), NPP variations appear mainly in the western and central portions of the study area with values ranging between 0 and 50 g C/m^2, and these two areas collectively account for 72.89% of the total study area. Under the warming scenario of 2.0 °C, the NPP increases in the west but decreases in the east. Regions with decreased NPP are distributed mainly in the northeast, accounting for 27.44% of the total study area. Under the 2.0 °C warming scenario, the main range of NPP variation is 100–300 g C/m^2. Of the regions exhibiting such increases, the SMSF in the central and western regions is the most significant ($P < 0.01$), accounting for 32.07% of the study area.

The spatial WUE variations are consistent with the NPP distributions under the two global warming scenarios (1.5 °C and 2.0 °C). Under the warming scenario of 1.5 °C (Fig. 2. e), the WUE values range predominantly from −0.2 to 0.2 g C/kg H_2O; the regions showing values within this range are distributed mainly in the SMSF in the western and central parts of the study area, accounting for approximately 70.03% of the total study area. Under the warming scenario of 2.0 °C (Fig. 2. f), the spatial variation in the WUE shows an increasing trend in the southeast and a decreasing trend in the northwest. The main range of increase in the east is 0.2–0.6 g C/kg H_2O, accounting for 33.11% of the total study area, while the main range of decrease in the west is −0.6–0.2 g C/kg H_2O, accounting for 30.63% of the total study area.

3.2. Temporal variability of ETa, NPP, and WUE

To study the *ETa,* NPP and WUE variations throughout the sandy areas of northern China, the interannual variabilities of the *ETa*, NPP and WUE under the four emission scenarios with RCPs (2006–2100) of 2.6, 4.5, 6.0 and 8.5 were inspected and then compared with their corresponding interannual variabilities during the reference period (1986–2005) (Fig. 3). Upward trends (Fig. 3. a) are observed in the overall *ETa* of all four emission scenarios. In comparison with the reference period, RCP6.0 shows the smallest increase (3.68%), while RCP8.5 shows the largest increase (6.48%) (Fig. 3. b). The reason may be due to the increasing of radiative forcing, there are some differences in response of surface vegetation to it (Andrews et al., 2012; Carrer et al., 2018; Thomson et al., 2011).When the radiative forcing reached the stable threshold of vegetation growth, the ET and NPP of vegetation showed an increasing trend. However, when the threshold was exceeded, the ET and NPP of vegetation showed a downward trend (Andrews et al., 2012; Davin et al., 2007; Luyssaert et al., 2011; Piao et al., 2008; Pinder et al., 2013). Therefore, RCP6.0 is different from the other RCPs. Compared with the reference period, the changes in *ETa* under the global warming scenarios of 1.5 °C and 2.0 °C are different to some extent with increases of 2.78% and 5.74%, respectively.

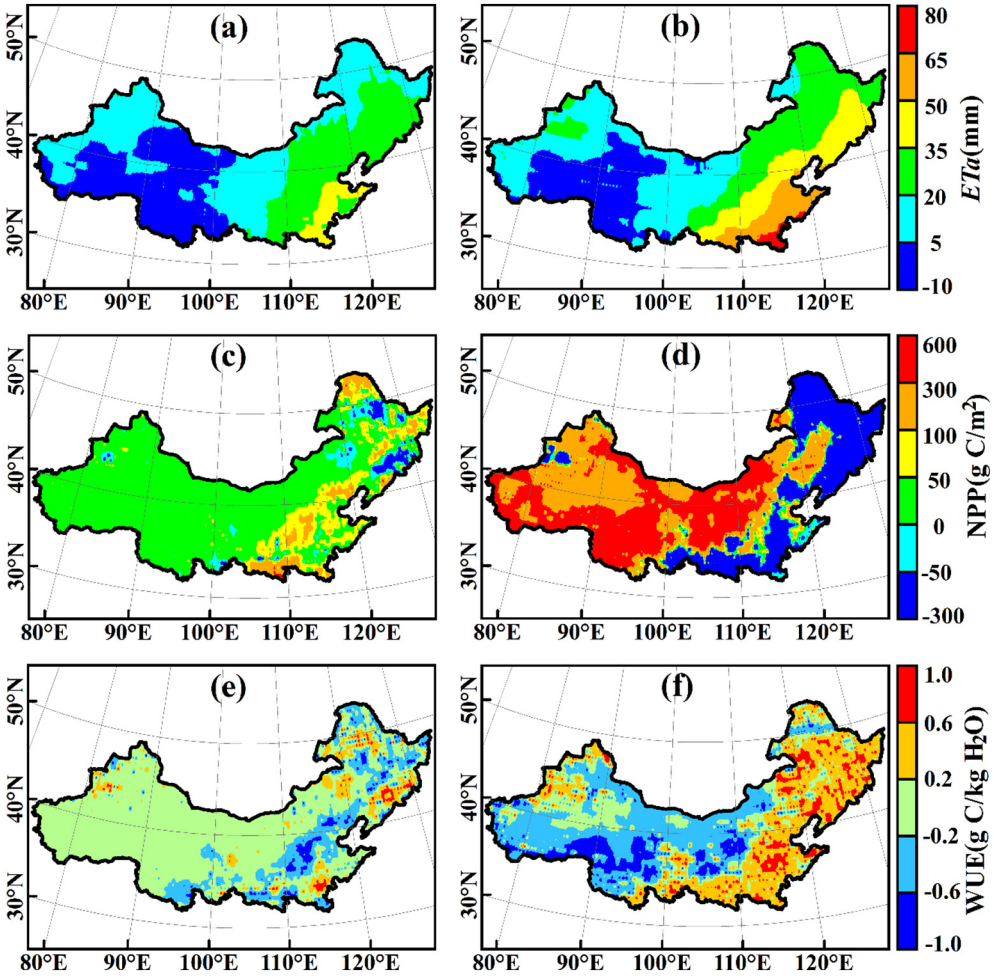

Fig. 2. The spatial patterns of *ETa*, NPP and WUE in the sandy areas of northern China under the global warming scenarios of 1.5 °C (a, c, e) and 2.0 °C (b, d, f) relative to the reference period (1986–2005).

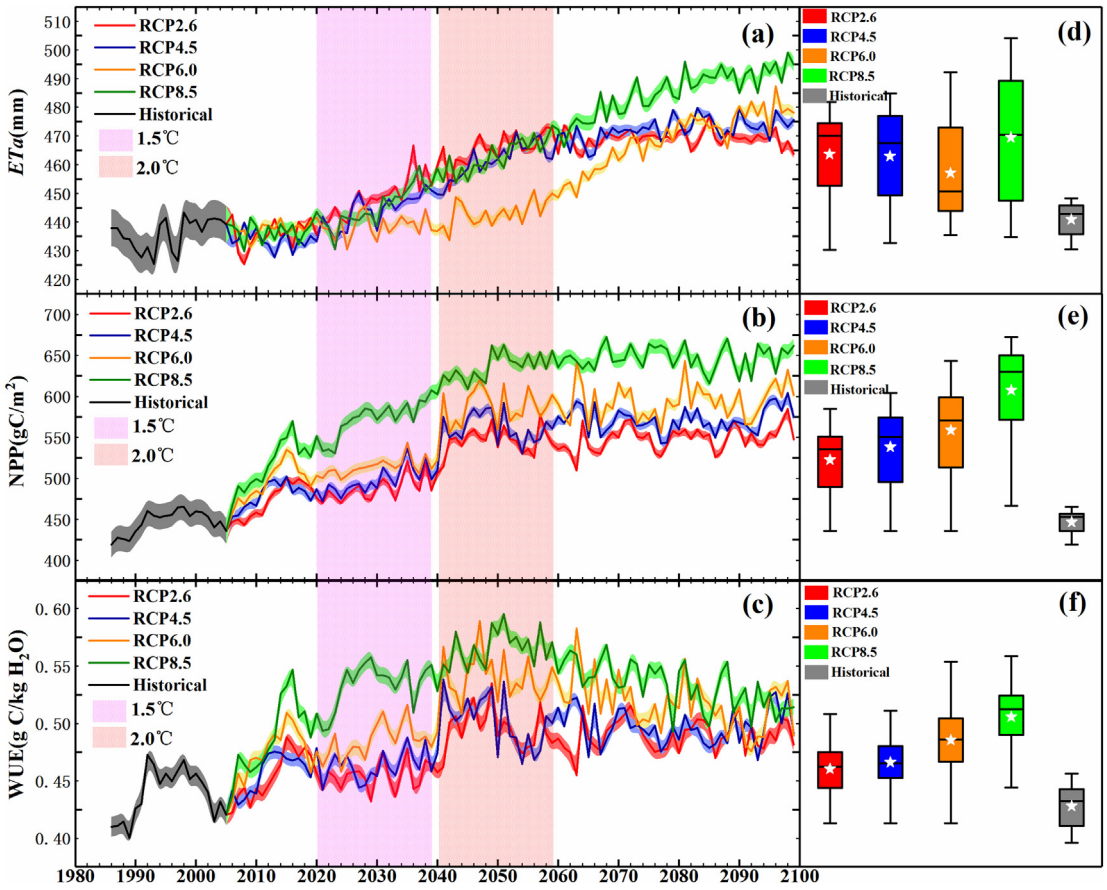

Fig. 3. Temporal variations in the *ETa*, NPP, and WUE values from 1986 to 2100. The horizontal lines in each boxplot represent the minimum, 25th percentile, median, 75th percentile and maximum of *ETa*/NPP/WUE from bottom to top, and the stars represent the *ETa*, NPP, and WUE averages.

Generally, the temperature and *ETa* variations are directly related, that is, *ETa* increases by 2.96% following a temperature increase from 1.5 °C to 2.0 °C relative to the reference period.

The future changes in NPP under the four RCPs and the emission concentrations demonstrate a positive correlation. In the period of 1986–2100, the trend of the overall NPP content increases under all four RCPs, that is, the NPP content increases by 128.32 g C/m^2 a, 156.02 g C/m^2 a, 182.47 g C/m^2 a and 242.67 g C/m^2 a under RCP2.6, RCP4.5, RCP6.0 and RCP8.5, respectively, relative to the conditions in 1986. The NPP content increases significantly in 2006–2029 and 2037–2042 but stabilizes after 2050. Under the warming scenarios of 1.5 °C and 2.0 °C, NPP increases by 8.57% and 24.01%, respectively, relative to the reference period. NPP increases less under the warming scenario of 1.5 °C than under the warming scenario of 2.0 °C with a 15.44% smaller increase relative to the reference period.

During different periods in the future, the WUE values in the sandy areas of northern China will first increase and then decrease with an overall increase compared with the reference period. The increase is greatest under RCP8.5 (23.97%) compared to 1986. Under the warming scenarios of 1.5 °C and 2.0 °C, the WUE variations will be 0.46–0.50 g C/kg H_2O and 0.49–0.55 g C/kg H_2O, respectively, representing increases of 3.44% and 13.51% compared with the reference period. Moreover, the WUE value increases by 10.07% with an additional temperature increase of 0.5 °C.

3.3. Comparison of the WUE variabilities under global warming scenarios of 1.5 °C and 2.0 °C

The spatial distributions of the WUE and its change rates were identified for various types of sandy land. Fig. 4 shows the spatial variations in the WUE under warming scenarios of 1.5 °C and 2.0 °C relative to the reference period. Under the warming scenario of 1.5 °C, the entire study area can be divided into approximately equal areas of decreasing WUE (49.59%) and increasing WUE (42.83%). The northwestern part of the study area, which is composed mainly of SMSF and MSL, witnesses a decrease in the WUE value, while the eastern and central parts of the study area (mainly FSL) exhibit an increased WUE. A significant difference is observed in the spatial WUE variations under the warming scenarios of 1.5 °C and 2.0 °C ($P < 0.01$). Under a temperature increase of 2.0 °C, the WUE increases (38.68%) in the northwestern part of the study area and decreases (31.74%) in the northeast; 14.54% of the area experiences a significant increase, while 15.04% of the area experiences a significant decrease. The results show that with an increase in the temperature, the WUE sensitivity in the sandy areas of northern China will vary among the different regions. With a continuous increase in the temperature in the arid areas of northwestern China, the WUE will increase further; among the three types of sandy land, FSL will show the most significant increase.

The WUE value shows a downward trend with increasing temperature in the MSL under the warming scenarios of 1.5 °C and 2.0 °C (Fig. 5). An increase in the global temperature of 0.5 °C induces a decrease in the WUE of MSL by 6.40%. In contrast, SMSF and FSL show increasing trends, with SMSF featuring the greatest increase (17.54%). WUE is closely related to the vegetation and climatic conditions of different sandy lands (Zhang et al., 2016). Global warming may lead to a decrease in the annual average precipitation and an increase in the number of extreme drought events in arid regions in the future (Su et al., 2018). However, in China, MSL is distributed mainly in arid and extremely arid regions, while SMSF and FSL are distributed in arid and semiarid regions; consequently, the degree of drought in MSL is relatively high, and the WUE of vegetation is diminished.

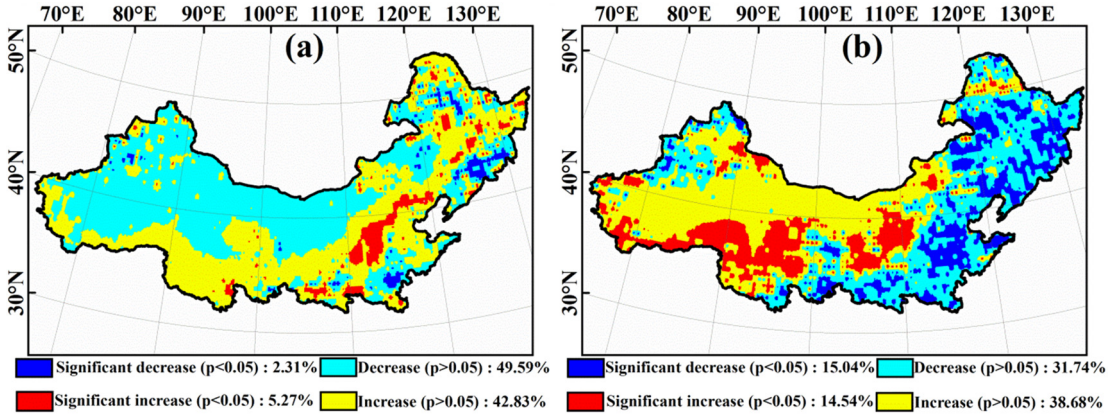

Fig. 4. Spatial distribution of the WUE changes under global warming scenarios of 1.5 °C (a) and 2.0 °C (b) relative to the reference period (1986–2005).

4. Discussion

4.1. Credibility of results

The carbon-water cycles in ecosystems are tightly coupled at many scales. WUE plays an important role in limiting plant growth, and its effect covers >40% of terrestrial ecosystems. Moreover, another 33% of terrestrial ecosystems lack water due to low temperatures (Tian et al., 2010). To understand the coupling of the carbon-water cycles in an ecosystem, it is necessary to consider WUE (Tian et al., 2010; Yu et al., 2008). Increasingly severe global warming may promote the growth of vegetation at high latitudes and high altitudes that are otherwise limited by insufficient heat. However, in most areas, an increase in the temperature may exacerbate aridification and weaken the carbon budget and WUE of vegetation (Mu et al., 2011a). Thus, climate change has led researchers to increasingly focus on the WUE of natural ecosystems such as wetlands, forests and grasslands; however, studies on the WUE of desert ecosystems remain limited (Table 3).

To date, WUE has been calculated mainly through the vorticity correlation method, the use of MODIS products and the ecosystem process model. Huang et al. (2017) studied the global distribution of WUE values (GPP (gross primary productivity)/ET) for the period of 2000–2014 using MODIS data and showed that tropical rainforests have high WUE values (4.0 g C kg^{-1} H_2O), while deserts have low WUE values (0.5 g C kg^{-1} H_2O). The spatial variations in WUE are also due to differences in the terrain and the data used (Tan et al., 2015).

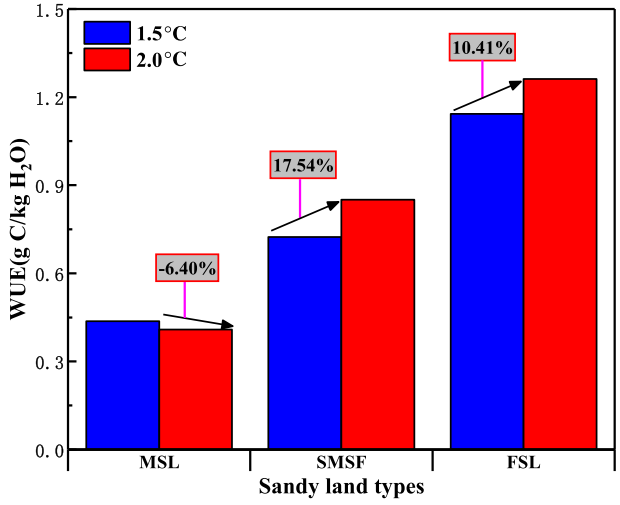

Fig. 5. Differences in the WUE among the diverse types of sandy land in northern China under the global warming scenarios of 1.5 °C and 2.0 °C.

For example, Liu et al. (2015) and Gao et al. (2014) evaluated the WUE in terrestrial ecosystems throughout China by using flux-site data and MODIS series data; they obtained average values of 0.79 g C kg^{-1} H_2O and 0.84 g C kg^{-1} H_2O, respectively. Furthermore, large differences were also encountered with the same data and the methodology for calculating the WUE of different vegetation types. For instance, Yu et al. (2008) and Hu et al. (2008) evaluated the WUE of both sandy and forest vegetation types using flux-site data and obtained results of 2.34 g C kg^{-1} H_2O and 0.46 g C kg^{-1} H_2O, respectively. However, even under the same vegetation type, the WUE exhibits considerable interstudy variability. Huang et al. (2017) estimated the WUE in Xinjiang (1979–2012) using the Biome-BGC (biogeochemical cycles) model and estimated the sandy land WUE to be 0.42 g C kg^{-1} H_2O, lower than that reported by Hu et al. (2008). This difference may have arisen because the desert ecosystem in Xinjiang is located in arid and extremely arid regions with little precipitation and few differences among vegetation types.

In summary, research on the WUE of an ecosystem features a relatively short timescale and is conducted mostly at the site scale. In the present study, the WUE values of sandy regions in northern China from 1986 to 2100 were estimated using ISIMIP2b model data with a calculated average of 0.48 g C kg^{-1} H_2O, higher than the results obtained by both Huang et al. (2017) and Hu et al. (2008). This discrepancy may exist because the climate model data used in the present study are based on data products under different emission paths, and an increase in the CO_2 concentration can promote a gradual increase in WUE over time (Knapp and Soule, 2011; Nock et al., 2011).

4.2. Meteorological factors associated with WUE variations under the global warming scenarios of 1.5 °C and 2.0 °C

The spatial distributions of the WUE values and change rates were identified for the three different types of sandy land (Fig. 6). Under the global warming scenarios of 1.5 °C and 2.0 °C, significant regional variability in the temperature rise is evident (Schaeffer et al., 2012; Su et al., 2017). In this context, except for the Hulunbuir and Horqin sandy lands at high latitudes (42–50°N), the temperature increases experienced by the sandy areas of northern China exceed 1.5 °C and 2.0 °C. The correlation between the WUE and temperature is negative for the different types of sandy land except for MSL. At the same time, the correlations between the WUE and temperature for the different types of sandy land under the warming scenario of 2.0 °C are all greater than those under the warming scenario of 1.5 °C, consistent with the findings of Zhang et al. (2013). This pattern may occur because temperature has a greater effect on photosynthesis than ET. However, Law et al. (2002) and Ponton et al. (2006) estimated the WUE of forestland using the eddy covariance technique and found that the WUE decreases with increasing temperature; this result may have occurred because the rate of increase

Table 3
Comparison among the simulated WUE values and those of published studies.[a]

Data	Methods	Study period	Location	WUE	References
MODIS data	WUE = GPP/ET	2000–2014	Global	1.70	Huang et al. (2017)
MODIS data	BEPS model	1982–2006	East Asia	1.58	Zhang et al. (2014)
Meteorological data	WUE = NPP/ET				
Flux-site data	WUE = GPP/ET	2001–2010	China	0.84	Gao et al. (2014)
MODIS data	BEPS model	2000–2011	China	0.79	Liu et al. (2015)
	WUE = NPP/ET				
Flux-site data	WUE = GPP/ET	2000–2008	Northern China	0.46	Hu et al. (2008)
Flux-site data	WUE = GPP/ET	2000–2006	Eastern China	2.34	Yu et al. (2008)
MODIS data	CASA model	2000–2010	Loess Plateau	0.98	Zhang et al. (2016)
Meteorological data	WUE = NPP/ET				
Meteorological data	Biome-BGC model	1979–2012	Xinjiang	0.42	Huang et al. (2018)
vegetation data	WUE = NPP/ET				
ISIMIP 2b data	AA model	1986–2099	Northern China	0.48	This study
	WUE = NPP/ET				

[a] GPP, gross primary production; BEPS, boreal ecosystem productivity simulator; Biome-BGC, biome biogeochemical cycle.

of ET is greater than that of NPP in forests at higher temperatures (Yu et al., 2008). However, Li et al. (2016) evaluated the NPP and ET of the global terrestrial ecosystem from 2000 to 2014 based on MODIS data and showed that with global warming, NPP presents a slightly increasing trend, but ET exhibits a significant increase, resulting in a slight increasing trend of the WUE. This is consistent with the results of our study. Global warming and vegetation greening accelerate ET in soil moisture, thus reducing the amount of soil water storage (Cox et al., 2013). The continuation of these trends will likely exacerbate drought in our study area. Under both global warming scenarios (1.5 °C and 2.0 °C), the precipitation decreases gradually from east to west, but it still increases relative to the reference period. Different regions show different ranges of increased precipitation; the main ranges are 0–10 mm and 10–20 mm. The precipitation of FSL under a warming of 2.0 °C is negatively correlated with WUE, while the precipitation amounts of other sandy land types (MSL and SMSF) are positively correlated with WUE, particularly in MSL. Under the warming scenario of 2.0 °C, the correlations between the precipitation amounts of the three types of sandy land and the WUE value of precipitation for all three types of sandy land are smaller than those under the warming scenario of 1.5 °C. These findings indicate that precipitation is not the main factor of global warming leading to the WUE variations in the study area. This lack of correlation may be related to the increase in the frequency of precipitation (Thomey et al., 2011) or the lag effect of precipitation (Sala et al., 2012).

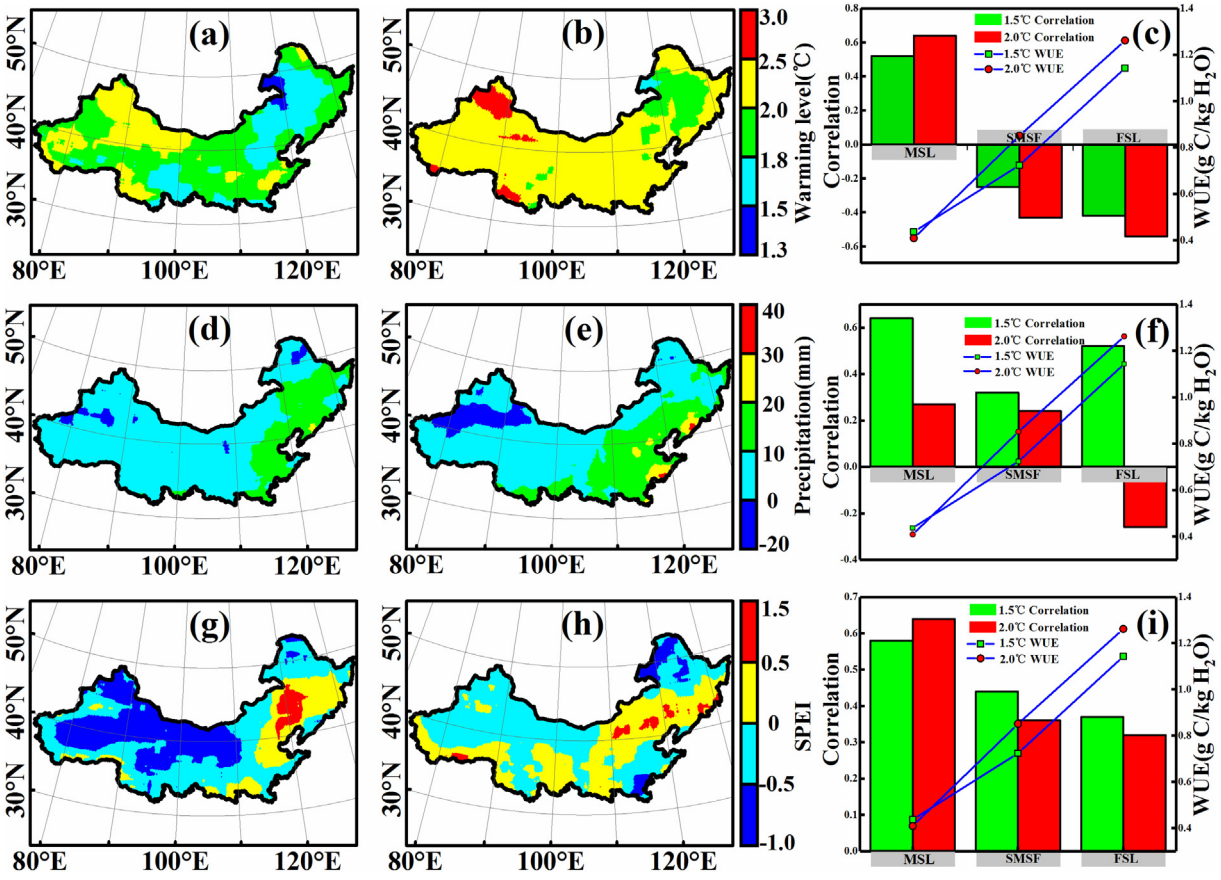

Fig. 6. Spatial distributions of the changes in the temperature, precipitation, and SPEI under the global warming scenarios of 1.5 °C (a, d, g) and 2.0 °C (b, e, h) in the sandy areas of northern China. In the bar and line charts, the bars represent the correlations between the meteorological factors and WUE under different types of sandy land (c: temperature and WUE; f: precipitation and WUE; i: SPEI and WUE), while the lines represent the WUE of different types of sandy land.

Precipitation and temperature are capable of reflecting the hydrothermal conditions of plant growth; these conditions influence the WUE in a complex and comprehensive way (Yu et al., 2008). In turn, WUE can reflect the water exchange balance on Earth (Hu et al., 2008; Yu et al., 2008). Global warming aggravates the degree of drought in China (Su et al., 2018), causing drought stress in plants (Davies, 2014) and increasing WUE to adapt to drought conditions (D. Liu et al., 2018). The SPEI was selected to study its relationship with WUE (Fig. 6. i); as a result, the spatial variations in the SPEI are reflected in Fig. 6. g and h in the context of global temperature increases of 1.5 °C and 2.0 °C, respectively. Under the warming scenarios of 1.5 °C and 2.0 °C, the SPEI tends to be spatially consistent in the northwestern portion but dry in the southeastern portion of the study area, consistent with the results of Wang et al. (2015). Generally positive correlations between the WUE and SPEI are evident for different types of sandy land, with MSL being the most significant. By studying the WUE responses of arid/semiarid ecosystems to drought, Zhang et al. (2016) found that WUE has a significant correlation with drought in arid regions. However, Hu et al. (2008) noted differences in the response period of WUE to drought. An analysis of the monthly SPEI of the sandy areas of northern China from 1981 to 2100 (Fig. S2) reveals that the SPEI ranges from −2.54 to 1.68, and the period of drought is concentrated mainly during May of each year.

4.3. Dynamics of the LAI and WUE

The LAI is an important parameter for certain global and regional ET and photosynthesis models (Bonan, 1993). An increase in the LAI not only effectively enhances the light use efficiency but also effectively inhibits soil water evaporation, which is a key influencing factor in the study of WUE (Tong et al., 2009). Our investigation of the LAI shows that temporal changes in the historical WUE in northern China are consistent with the variations in the LAI, and the two parameters exhibit a strongly linear relationship: $LAI = -0.75 + 5.32 \times WUE - 5.33 \times (WUE)^2$. When LAI decreases, the WUE value increases. However, when the LAI decreases to 0.54 $m^2\ m^{-2}$, the range of variability of both the WUE and the LAI is narrow. This pattern may exist because the effective area of the canopy intercepting light energy increases rapidly when the LAI is small, and the evaporation of water from the underlying soil decreases with an increase in the LAI (Li et al., 2004a; Wang et al., 2007a; Wang et al., 2007b), which causes the WUE to increase rapidly. However, when the LAI decreases below a certain threshold, the variation in the surface area of the canopy effectively intercepting light energy is not significant (Muraoka et al., 2010); thus, variations in the LAI and WUE tend to be minor. The increase in the LAI of sandy lands under the global warming scenario of 1.5 °C is remarkably greater than that under the global warming scenario of 2 °C, a possible reason for which is the withering of sand-fixing vegetation (Li et al., 2017; Li et al., 2013b) and the decrease in the LAI with warming due to the further aggravation of aridification under increased warming (Fig 7).

4.4. Response of desertification to WUE

According to the United Nations Convention to Combat Desertification, desertification includes the degeneration of land in subhumid, semiarid and arid regions caused by many factors, such as anthropogenic activities and climate change (National Strategy for Sustainable Development and UNEP, 1994). This convention also adopted a target to achieve land degradation neutrality by 2030 (Reid et al., 2017). The variation in the extent of sandy areas is a key indicator of desertification (Ma et al., 2018; Reynolds et al., 2007), and monitoring desertification is of particular importance for tracking its effects on the eco-environment and social economy of the arid regions in northern China, especially because China is among the nations suffering from the most serious desertification worldwide (Wang et al., 2013; Zhang et al., 2018).

The WUE value not only reflects the water consumption of vegetation but also demonstrates the adaptability of vegetation to drought (Ito and Inatomi, 2012). Variations in the extents of sandy areas not only directly reflect the growth of sand-fixing vegetation but also indicate the advantages and disadvantages of the eco-environment in the desert. Therefore, the extent of desertification in the sandy areas of northern China was explored by establishing the relationship between the sandy area extent and WUE (Fig. 8). During the historical period (1986–2015), the extent of sandy areas in northern China showed a generally decreasing trend (−6.6 km^2 per decade). In addition, the sandy area extent in northern China demonstrates a strongly linear relationship with the WUE ($R^2 = 0.76$): $Sandy\ Area = -6305.82 + 23{,}294.46 \times WUE - 20{,}890.44 \times (WUE)^2$. The future extent of sandy areas in northern China exhibits large fluctuations (2016–2047), followed by a gradual increase (2047–2100). The extent of sandy areas under RCP2.6 is lower than that under RCP4.5. From 2016 to 2047, the extents of sandy areas under RCP2.6 and RCP4.5 are projected to increase by 22.63×10^4 km^2 per decade and 22.35×10^4 km^2 per decade, respectively, while the sandy area extents under these two emission scenarios are projected to increase by only 2.60×10^4 km^2 per decade and 3.65×10^4 km^2 per decade, respectively, after 2047. The aforementioned results indicate that the increase rate of the sandy area extent in northern China after approximately 2050 are minor is smaller compared to before 2050, possibly due to the maturation of the internal development of sandy ecosystems over time (Wang et al., 2007b) and the evolution of the type of sandy area from MSL to FSL. Biological soil crust (BSC) is an integral part of the soil system in arid regions, stabilizing soil surfaces, aiding vascular plant establishment, and promoting the carbon-water cycle in sandy lands (Grote et al., 2010). Therefore, the emergence of BSC (Belnap and Gillette, 1998; Li et al., 2014; Zhao et al., 2011) will, to a certain extent, prevent the process of desertification (Li et al., 2017; Shi et al., 2018). There is an obvious difference between the extents of the sandy areas in northern China under the warming scenarios of 1.5 °C and 2.0 °C; the extent of sandy area under the warming scenario of 2.0 °C is 40.06% (50.33×10^4 km^2) greater than that under the warming scenario of 1.5 °C. This finding indicates that global warming might aggravate the desertification of the sandy areas in northern China to some extent.

5. Conclusions

In this study, the CASA and AA models were used to estimate the WUE (NPP/*ETa*) in sandy areas throughout northern China under global warming scenarios of 1.5 °C and 2.0 °C using ISIMIP2b datasets. Simulations were compared against data from eddy covariance towers located in different types of sandy land, thereby confirming the reliability of our model estimates. The results showed that the coupled carbon-water cycle in the study area was reflected well by the results of the selected model. Compared with the reference period (1986–2005), the *ETa*, NPP, and WUE increased by 2.96%, 15.44% and 10.07%, respectively, from a global warming scenario of 1.5 °C to a global warming scenario of 2.0 °C, and these three parameters showed gradually increasing trends from southeast to northwest. The average WUE was 0.48 g C/kg H_2O from 1986 to 2100, and the highest WUE values were distributed mostly in FSL.

The WUE values showed appreciable differences among the three types of sandy land under the global warming scenarios of 1.5 °C and 2.0 °C. The WUE value in MSL decreased by 6.40% when the global temperature rose from 1.5 °C to 2.0 °C, while the WUE values in SMSF and FSL showed increasing trends, with SMSF showing the most significant increase (17.54%). We found that the significant spatiotemporal differences in WUE were caused mainly by its interactions with various meteorological factors (precipitation, temperature and SPEI) and with the LAI under global warming scenarios of 1.5 °C and 2.0 °C. Under the global warming scenarios of 1.5 °C and 2.0 °C, the warming in all the sandy areas except for the Hulunbuir

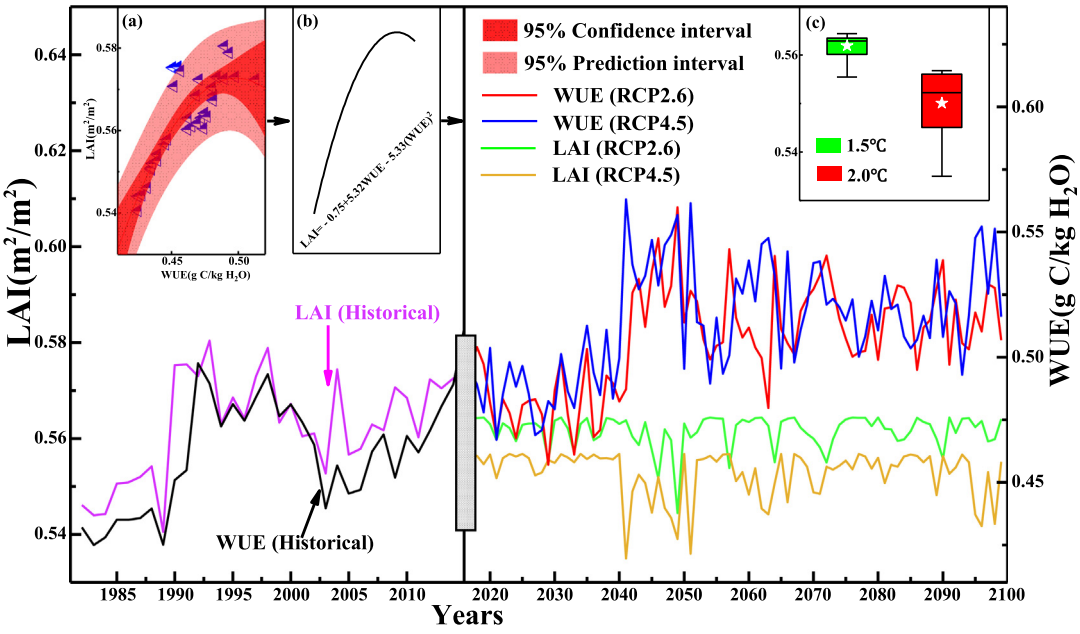

Fig. 7. Relationship between the annual average LAI and WUE from 1981 to 2100 in the sandy areas of northern China (a: fitting the historical LAI and WUE; b: fitting curve; c: LAI boxplot under the global warming scenarios of 1.5 °C and 2.0 °C). The horizontal lines in the boxplots represent the minimum, 25th percentile, median, 75th percentile and maximum LAI values from bottom to top, and the stars represent the average LAI value.

and Horqin sandy lands at high latitudes (42°-52° N) reached and exceeded 1.5 °C and 2.0 °C. The precipitation and SPEI also showed a decreasing trend from east to west. The correlations with the WUE under different meteorological conditions were better for MSL than for the other sandy land types. We found that the only correlation to decrease among the three sandy lands under the influence of global warming was that between the precipitation and WUE. This finding indicates that precipitation is not the dominant factor influencing changes in the WUE in the study area. The fluctuations in the WUE over time are consistent with those of the LAI in the sandy lands of northern China. The LAI is clearly lower under the global warming scenario of 2.0 °C than under the global warming scenario of 1.5 °C.

The degree of desertification comprehensively reflects the relationships among the SPEI, LAI and WUE. In the future, the extent of sandy areas will increase by an average of 20×10^4 km^2 per decade (2016–2047) but will slow (2.60×10^4 km^2 per decade) after 2050 (2050–2100). Therefore, the earlier implementation of a 1.5 °C warming target will further reduce the risk of desertification, and this target is conducive to the coordinated development of the environment and social economy in the Silk Road Economic Belt.

Acknowledgments

The authors of this study would like to express their appreciation to the key project of the National Natural Science Foundation of China

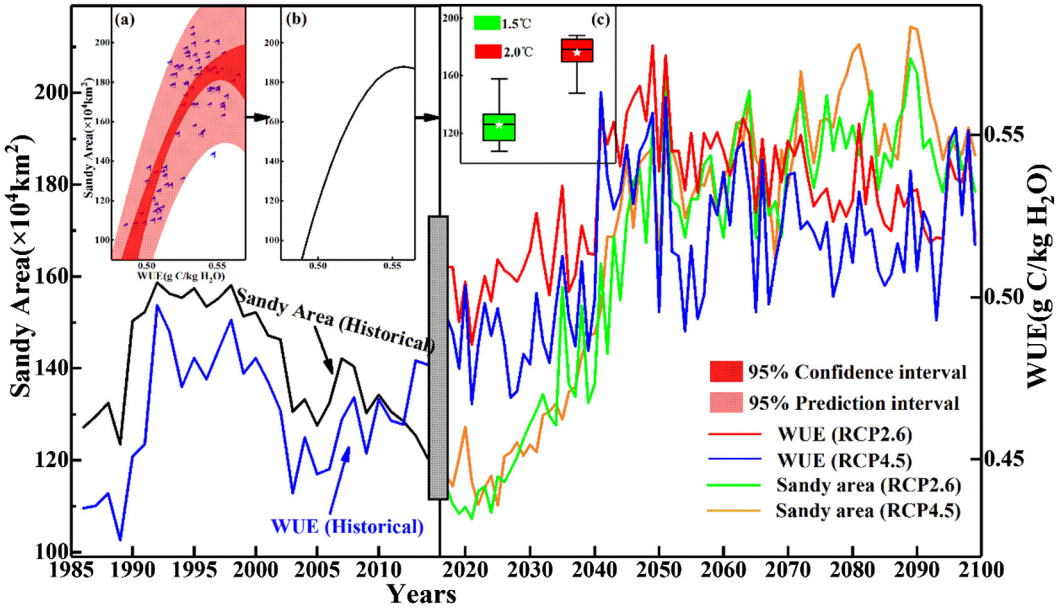

Fig. 8. Relationship between the extent of sandy areas and WUE from 1980 to 2100 in the sandy areas of northern China (a: fitting the historical sandy areas and WUE; b: fitting curve; c: boxplots of the sandy area extent under the global warming scenarios of 1.5 °C and 2.0 °C). The horizontal lines in the boxplots represent the minimum, 25th percentile, median, 75th percentile and maximum sandy area values from bottom to top, and the stars represent the average sandy area extent.

(41671030, U1403281), the Natural Science Foundation of Jiangsu Province (BK20181059), the National Basic Research Program of China (2013CB429905) and the project of Thousand Young Talents Program (Y772121) for their sponsorship. They would also like to show their appreciation to CERN (China Ecosystem Research Network) and ChinaFLUX (China FLUX Observation and Research Network) for the observation data from the Aksu, Tazhong, Fukang, Shapotou, Yanchi and Naiman stations.

Conflicts of interest

The authors declare that they have no conflicts of interest.

Special issue statement

This article is part of the special issue "Ecosystems, climate and land-use change across Asia and Australasia an OzFlux–Asiaflux."

Appendix A. Supplementary data

Supplementary data to this article can be found online at https://doi.org/10.1016/j.scitotenv.2019.01.402.

References

Andrews, T., Ringer, M.A., Doutriaux-Boucher, M., Webb, M.J., Collins, W.J., 2012. Sensitivity of an Earth system climate model to idealized radiative forcing. Geophys. Res. Lett. 39, 6.

Baldocchi, D., 1994. A comparative-study of mass and energy-exchange rates over a closed C-3 (wheat) and an open C-4 (corn) crop. 2. CO_2 exchange and water-use efficiency. Agric. For. Meteorol. 67 (3–4), 291–321.

Battipaglia, G., De Micco, V., Brand, W.A., Saurer, M., Aronne, G., Linke, P., Cherubini, P., 2014. Drought impact on water use efficiency and intra-annual density fluctuations in Erica arborea on Elba (Italy). Plant Cell Environ. 37 (2), 382–391.

Belnap, J., Gillette, D.A., 1998. Vulnerability of desert biological soil crusts to wind erosion: the influences of crust development, soil texture, and disturbance. J. Arid Environ. 39 (2), 133–142.

Bonan, G.B., 1993. Importance of leaf-area index and forest type when estimating photosynthesis in boreal forests. Remote Sens. Environ. 43 (3), 303–314.

Brutsaert, W., Stricker, H., 1979. Advection-aridity approach to estimate actual regional evapotranspiration. Water Resour. Res. 15 (2), 443–450.

Carrer, D., Pique, G., Ferlicoq, M., Ceamanos, X., Ceschia, E., 2018. What is the potential of cropland albedo management in the fight against global warming? A case study based on the use of cover crops. Environ. Res. Lett. 13 (4), 11.

Cox, P.M., Pearson, D., Booth, B.B., Friedlingstein, P., Huntingford, C., Jones, C.D., Luke, C.M., 2013. Sensitivity of tropical carbon to climate change constrained by carbon dioxide variability. Nature 494 (7437), 341–344.

Davies, W.J., 2014. Exploiting plant drought stress biology to increase resource use efficiency and yield of crops under water scarcity. Theor. Exp. Plant Physiol. 26 (1), 1–3.

Davin, E.L., de Noblet-Ducoudre, N., Friedlingstein, P., 2007. Impact of land cover change on surface climate: relevance of the radiative forcing concept. Geophys. Res. Lett. 34 (13), 5.

Dong, C.Y., Wang, N.A., Chen, J.S., Li, Z.L., Chen, H.B., Chen, L., Ma, N., 2016. New observational and experimental evidence for the recharge mechanism of the lake group in the Alxa Desert, north-central China. J. Arid Environ. 124, 48–61.

Du, H., Wang, T., Xue, X., Li, S., 2018. Modelling of sand/dust emission in Northern China from 2001 to 2014. Geoderma 330, 162–176.

Duan, Z.H., Xiao, H.L., Dong, Z.B., He, X.D., Wang, G., 2001. Estimate of total CO_2 output from desertified sandy land in China. Atmos. Environ. 35 (34), 5915–5921.

Fawcett, A.A., Iyer, G.C., Clarke, L.E., Edmonds, J.A., Hultman, N.E., McJeon, H.C., Rogelj, J., Schuler, R., Alsalam, J., Asrar, G.R., Creason, J., Jeong, M., McFarland, J., Mundra, A., Shi, W.J., 2015. Can Paris pledges avert severe climate change? Science 350 (6265), 1168–1169.

Field, C.B., Randerson, J.T., Malmstrom, C.M., 1995. Global net primary production: combining ecology and remote sensing. Remote Sens. Environ. 51 (1), 74–88.

Fischer, R.A., Turner, N.C., 1978. Plant productivity in arid and semi-aris zones. Annu. Rev. Plant Physiol. Plant Mol. Biol. 29, 277–317.

Friedl, M.A., Sulla-Menashe, D., Tan, B., Schneider, A., Ramankutty, N., Sibley, A., Huang, X.M., 2010. MODIS collection 5 global land cover: algorithm refinements and characterization of new datasets. Remote Sens. Environ. 114 (1), 168–182.

Frieler, K., Lange, S., Piontek, F., Reyer, C.P.O., Schewe, J., Warszawski, L., Zhao, F., Chini, L., Denvil, S., Emanuel, K., Geiger, T., Halladay, K., Hurtt, G., Mengel, M., Murakami, D., Ostberg, S., Popp, A., Riva, R., Stevanovic, M., Suzuki, T., Volkholz, J., Burke, E., Ciais, P., Ebi, K., Eddy, T.D., Elliott, J., Galbraith, E., Gosling, S.N., Hattermann, F., Hickler, T., Hinkel, J., Hof, C., Huber, V., Jagermeyr, J., Krysanova, V., Marce, R., Schmied, H.M., Mouratiadou, I., Pierson, D., Tittensor, D.P., Vautard, R., van Vliet, M., Biber, M.F., Betts, R.A., Bodirsky, B.L., Deryng, D., Frolking, S., Jones, C.D., Lotze, H.K., Lotze-Campen, H., Sahajpal, R., Thonicke, K., Tian, H.Q., Yamagata, Y., 2017. Assessing the impacts of 1.5 degrees C global warming - simulation protocol of the Inter-Sectoral Impact Model Intercomparison Project (ISIMIP2b). Geosci. Model Dev. 10 (12), 4321–4345.

Fu, Y.L., Yu, G.R., Sun, X.M., Li, Y.N., Wen, X.F., Zhang, L.M., Li, Z.Q., Zhao, L., Hao, Y.B., 2006. Depression of net ecosystem CO_2 exchange in semi-arid Leymus chinensis steppe and alpine shrub. Agric. For. Meteorol. 137 (3–4), 234–244.

Gang, C.C., Wang, Z.Q., Chen, Y.Z., Yang, Y., Li, J.L., Cheng, J.M., Qi, J.G., Odeh, I., 2016. Drought-induced dynamics of carbon and water use efficiency of global grasslands from 2000 to 2011. Ecol. Indic. 67, 788–797.

Gao, Y., Zhu, X.J., Yu, G.R., He, N.P., Wang, Q.F., Tian, J., 2014. Water use efficiency threshold for terrestrial ecosystem carbon sequestration in China under afforestation. Agric. For. Meteorol. 195, 32–37.

Grote, E.E., Belnap, J., Housman, D.C., Sparks, J.P., 2010. Carbon exchange in biological soil crust communities under differential temperatures and soil water contents: implications for global change. Glob. Chang. Biol. 16 (10), 2763–2774.

Hao, C., Wu, S., 2006. The effects of land-use types and conversions on desertification in Mu Us Sandy Land of China. J. Geogr. Sci. 16 (1), 57–68.

Haque, A., 2003. Estimating actual areal evapotranspiration from potential evapotranspiration using physical models based on complementary relationships and meteorological data. Bull. Eng. Geol. Environ. 62 (1), 57–63.

Hu, G.C., Jia, L., 2015. Monitoring of evapotranspiration in a semi-arid inland river basin by combining microwave and optical remote sensing observations. Remote Sens. 7 (3), 3056–3087.

Hu, Z.M., Yu, G.R., Fu, Y.L., Sun, X.M., Li, Y.N., Shi, P.L., Wangw, Y.F., Zheng, Z.M., 2008. Effects of vegetation control on ecosystem water use efficiency within and among four grassland ecosystems in China. Glob. Chang. Biol. 14 (7), 1609–1619.

Huang, M.T., Piao, S.L., Sun, Y., Ciais, P., Cheng, L., Mao, J.F., Poulter, B., Shi, X.Y., Zeng, Z.Z., Wang, Y.P., 2015. Change in terrestrial ecosystem water-use efficiency over the last three decades. Glob. Chang. Biol. 21 (6), 2366–2378.

Huang, L., He, B., Han, L., Liu, J.J., Wang, H.Y., Chen, Z.Y., 2017. A global examination of the response of ecosystem water-use efficiency to drought based on MODIS data. Sci. Total Environ. 601, 1097–1107.

Huang, X.T., Luo, G.P., Ye, F.P., Han, Q.F., 2018. Effects of grazing on net primary productivity, evapotranspiration and water use efficiency in the grasslands of Xinjiang, China. J. Arid. Land 10 (4), 588–600.

IPCC, 2013. Climate change 2013: the physical science basis. In: Stocker, T.F., Qin, D., Plattner, G.-K., Tignor, M., Allen, S.K., Boschung, J., Nauels, A., Xia, Y., Bex, V., Midgley, P.M. (Eds.), Contribution of Working Group I to the Fifth Assessment Report of the Intergovernmental Panel on Climate Change. Cambridge University Press, Cambridge, United Kingdom and New York, NY, USA 1535 pp.

Ito, A., Inatomi, M., 2012. Water-use efficiency of the terrestrial biosphere: a model analysis focusing on interactions between the global carbon and water cycles. J. Hydrometeorol. 13 (2), 681–694.

Jassal, R.S., Black, T.A., Spittlehouse, D.L., Brummer, C., Nesic, Z., 2009. Evapotranspiration and water use efficiency in different-aged Pacific Northwest Douglas-fir stands. Agric. For. Meteorol. 149 (6–7), 1168–1178.

Jian, D., Li, X., Sun, H., Tao, H., Jiang, T., Su, B., Hartmann, H., 2018. Estimation of actual evapotranspiration by the complementary theory-based advection–aridity model in the Tarim River Basin, China. J. Hydrometeorol. 19 (2), 289–303.

Jiao, L., Lu, N., Fu, B.J., Wang, J., Li, Z.S., Fang, W.W., Liu, J.B., Wang, C., Zhang, L.W., 2018. Evapotranspiration partitioning and its implications for plant water use strategy: evidence from a black locust plantation in the semi-arid Loess Plateau, China. For. Ecol. Manag. 424, 428–438.

Keenan, T.F., Hollinger, D.Y., Bohrer, G., Dragoni, D., Munger, J.W., Schmid, H.P., Richardson, A.D., 2013. Increase in forest water-use efficiency as atmospheric carbon dioxide concentrations rise. Nature 499 (7458) (324-+).

King, A.D., Karoly, D.J., Henley, B.J., 2017. Australian climate extremes at 1.5 degrees C and 2 degrees C of global warming. Nat. Clim. Chang. 7 (6) (412-+).

Knapp, P.A., Soule, P.T., 2011. Increasing water-use efficiency and age-specific growth responses of old-growth ponderosa pine trees in the Northern Rockies. Glob. Chang. Biol. 17 (1), 631–641.

Law, B.E., Falge, E., Gu, L., Baldocchi, D.D., Bakwin, P., Berbigier, P., Davis, K., Dolman, A.J., Falk, M., Fuentes, J.D., Goldstein, A., Granier, A., Grelle, A., Hollinger, D., Janssens, I.A., Jarvis, P., Jensen, N.O., Katul, G., Mahli, Y., Matteucci, G., Meyers, T., Monson, R., Munger, W., Oechel, W., Olson, R., Pilegaard, K., Paw, K.T., Thorgeirsson, H., Valentini, R., Verma, S., Vesala, T., Wilson, K., Wofsy, S., 2002. Environmental controls over carbon dioxide and water vapor exchange of terrestrial vegetation. Agric. For. Meteorol. 113 (1–4), 97–120.

Li, X.R., Ma, F.Y., Xiao, H.L., Wang, X.P., Kim, K.C., 2004a. Long-term effects of revegetation on soil water content of sand dunes in arid region of Northern China. J. Arid Environ. 57 (1), 1–16.

Li, X.R., Xiao, H.L., Zhang, J.G., Wang, X.P., 2004b. Long-term ecosystem effects of sand-binding vegetation in the Tengger Desert, northern China. Restor. Ecol. 12 (3), 376–390.

Li, J., Zhao, C., Zhu, H., Li, Y., Wang, F., 2007. Effect of plant species on shrub fertile island at an oasis–desert ecotone in the South Junggar Basin, China. J. Arid Environ. 71 (4), 350–361.

Li, X., Gemmer, M., Zhai, J., Liu, X., Su, B., Wang, Y., 2013a. Spatio-temporal variation of actual evapotranspiration in the Haihe River Basin of the past 50 years. Quat. Int. 304, 133–141.

Li, X.R., Zhang, Z.S., Huang, L., Wang, X.P., 2013b. Review of the ecohydrological processes and feedback mechanisms controlling sand-binding vegetation systems in sandy desert regions of China. Chin. Sci. Bull. 58 (13), 1483–1496.

Li, X.R., Gao, Y.H., Su, J.Q., Jia, R.L., Zhang, Z.S., 2014. Ants mediate soil water in arid desert ecosystems: mitigating rainfall interception induced by biological soil crusts? Appl. Soil Ecol. 78, 57–64.

Li, Z., Chen, Y.N., Wang, Y., Fang, G.H., 2016. Dynamic changes in terrestrial net primary production and their effects on evapotranspiration. Hydrol. Earth Syst. Sci. 20 (6), 2169–2178.

Li, X.R., Zhang, D.H., Zhang, F., Zhang, P., 2017. The eco-hydrological threshold for evaluating the stability of sand-binding vegetation in different climatic zones. Ecol. Indic. 83, 404–415.

Liang, W., Yang, Y.T., Fan, D.M., Guan, H.D., Zhang, T., Long, D., Zhou, Y., Bai, D., 2015. Analysis of spatial and temporal patterns of net primary production and their climate controls in China from 1982 to 2010. Agric. For. Meteorol. 204, 22–36.

Liu, Y.B., Xiao, J.F., Ju, W.M., Zhou, Y.L., Wang, S.Q., Wu, X.C., 2015. Water use efficiency of China's terrestrial ecosystems and responses to drought. Sci. Rep. 5, 12.

Liu, D., Yu, C.L., Zhao, F., 2018. Response of the water use efficiency of natural vegetation to drought in Northeast China. J. Geogr. Sci. 28 (5), 611–628.

Liu, Q.F., Zhao, Y.Y., Zhang, X.F., Buyantuev, A., Niu, J.M., Wang, X.J., 2018. Spatiotemporal patterns of desertification dynamics and desertification effects on ecosystem Services in the Mu Us Desert in China. Sustainability 10 (3), 19.

Loveland, T.R., Belward, A.S., 1997. The IGBP-DIS global 1 km land cover data set, DISCover: first results. Int. J. Remote Sens. 18 (15), 3291–3295.

Lu, X.L., Zhuang, Q.L., 2010. Evaluating evapotranspiration and water-use efficiency of terrestrial ecosystems in the conterminous United States using MODIS and AmeriFlux data. Remote Sens. Environ. 114 (9), 1924–1939.

Luyssaert, S., Hessenmoller, D., von Lupke, N., Kaiser, S., Schulze, E.D., 2011. Quantifying land use and disturbance intensity in forestry, based on the self-thinning relationship. Ecol. Appl. 21 (8), 3272–3284.

Ma, X., Zhao, C., Tao, H., Zhu, J., Kundzewicz, Z.W., 2018. Projections of actual evapotranspiration under the 1.5 °C and 2.0 °C global warming scenarios in sandy areas in northern China. Sci. Total Environ. 645, 1496–1508.

Mu, Q.Z., Zhao, M.S., Running, S.W., 2011a. Evolution of hydrological and carbon cycles under a changing climate. Part III: global change impacts on landscape scale evapotranspiration. Hydrol. Process. 25 (26), 4093–4102.

Mu, Q.Z., Zhao, M.S., Running, S.W., 2011b. Improvements to a MODIS global terrestrial evapotranspiration algorithm. Remote Sens. Environ. 115 (8), 1781–1800.

Muraoka, H., Saigusa, N., Nasahara, K.N., Noda, H., Yoshino, J., Saitoh, T.M., Nagai, S., Murayama, S., Koizumi, H., 2010. Effects of seasonal and interannual variations in leaf photosynthesis and canopy leaf area index on gross primary production of a cool-temperate deciduous broadleaf forest in Takayama, Japan. J. Plant Res. 123 (4), 563–576.

National Strategy for Sustainable Development, L.U.K.e, UNEP, N.K.e, 1994. United Nations Convention to Combat Desertification in Countries Experiencing Serious Drought and/or Desertification, Particularly in Africa.

Nock, C.A., Baker, P.J., Wanek, W., Leis, A., Grabner, M., Bunyavejchewin, S., Hietz, P., 2011. Long-term increases in intrinsic water-use efficiency do not lead to increased stem growth in a tropical monsoon forest in western Thailand. Glob. Chang. Biol. 17 (2), 1049–1063.

Pettorelli, N., Vik, J.O., Mysterud, A., Gaillard, J.M., Tucker, C.J., Stenseth, N.C., 2005. Using the satellite-derived NDVI to assess ecological responses to environmental change. Trends Ecol. Evol. 20 (9), 503–510.

Piao, S.L., Fang, J.Y., Zhou, L.M., Zhu, B., Tan, K., Tao, S., 2005. Changes in vegetation net primary productivity from 1982 to 1999 in China. Glob. Biogeochem. Cycles 19 (2), 19.

Piao, S.L., Ciais, P., Friedlingstein, P., Peylin, P., Reichstein, M., Luyssaert, S., Margolis, H., Fang, J.Y., Barr, A., Chen, A.P., Grelle, A., Hollinger, D.Y., Laurila, T., Lindroth, A., Richardson, A.D., Vesala, T., 2008. Net carbon dioxide losses of northern ecosystems in response to autumn warming. Nature 451 (7174), 49–52.

Pinder, R.W., Bettez, N.D., Bonan, G.B., Greaver, T.L., Wieder, W.R., Schlesinger, W.H., Davidson, E.A., 2013. Impacts of human alteration of the nitrogen cycle in the US on radiative forcing. Biogeochemistry 114 (1–3), 25–40.

Ponton, S., Flanagan, L.B., Alstad, K.P., Johnson, B.G., Morgenstern, K., Kljun, N., Black, T.A., Barr, A.G., 2006. Comparison of ecosystem water-use efficiency among Douglas-fir forest, aspen forest and grassland using eddy covariance and carbon isotope techniques. Glob. Chang. Biol. 12 (2), 294–310.

Potter, C.S., Randerson, J.T., Field, C.B., Matson, P.A., Vitousek, P.M., Mooney, H.A., Klooster, S.A., 1993. Terrestrial ecosystem production: a process model based on global satellite and surface data. Glob. Biogeochem. Cycles 7 (4), 811–841.

Reid, A.J., Brooks, J.L., Dolgova, L., Laurich, B., Sullivan, B.G., Szekeres, P., Wood, S.L.R., Bennett, J.R., Cooke, S.J., 2017. Post-2015 Sustainable Development Goals still neglecting their environmental roots in the Anthropocene. Environ. Sci. Pol. 77, 179–184.

Reynolds, J.F., Stafford Smith, D.M., Lambin, E.F., Turner, B.L., Mortimore, M., Batterbury, S.P.J., Downing, T.E., Dowlatabadi, H., Fernandez, R.J., Herrick, J.E., Huber-Sannwald, E., Jiang, H., Leemans, R., Lynam, T., Maestre, F.T., Ayarza, M., Walker, B., 2007. Global desertification: building a science for dryland development. Science 316 (5826), 847–851.

Sala, O.E., Gherardi, L.A., Reichmann, L., Jobbagy, E., Peters, D., 2012. Legacies of precipitation fluctuations on primary production: theory and data synthesis. Philos. Trans. R. Soc. Lond. Ser. B Biol. Sci. 367 (1606), 3135–3144.

Schaeffer, M., Hare, W., Rahmstorf, S., Vermeer, M., 2012. Long-term sea-level rise implied by 1.5 degrees C and 2 degrees C warming levels. Nat. Clim. Chang. 2 (12), 867–870.

Shi, W., Wang, X.P., Zhang, Y.F., Pan, Y.X., Hu, R., Jin, Y.X., 2018. The effect of biological soil crusts on soil moisture dynamics under different rainfall conditions in the Tengger Desert, China. Hydrol. Process. 32 (10), 1363–1374.

Singh, V.P., Guo, H., Yu, F.X., 1993. Parameter estimation for 3-parameter log-logistic distribution (LLD3) by Pome. Stoch. Hydrol. Hydraul. 7 (3), 163–177.

Stow, D., Daeschner, S., Hope, A., Douglas, D., Petersen, A., Myneni, R., Zhou, L., Oechel, W., 2003. Variability of the seasonally integrated normalized difference vegetation index across the north slope of Alaska in the 1990s. Int. J. Remote Sens. 24 (5), 1111–1117.

Su, B.D., Jian, D.N., Li, X.C., Wang, Y.J., Wang, A.Q., Wen, S.S., Tao, H., Hartmann, H., 2017. Projection of actual evapotranspiration using the COSMO-CLM regional climate model under global warming scenarios of 1.5 degrees C and 2.0 degrees C in the Tarim River basin, China. Atmos. Res. 196, 119–128.

Su, B.D., Huang, J.L., Fischer, T., Wang, Y.J., Kundzewicz, Z.W., Zhai, J.Q., Sun, H.M., Wang, A.Q., Zeng, X.F., Wang, G.J., Tao, H., Gemmer, M., Li, X.C., Jiang, T., 2018. Drought losses in China might double between the 1.5 degrees C and 2.0 degrees C warming. Proc. Natl. Acad. Sci. U. S. A. 115 (42), 10600–10605.

Sun, Y., Piao, S.L., Huang, M.T., Ciais, P., Zeng, Z.Z., Cheng, L., Li, X.R., Zhang, X.P., Mao, J.F., Peng, S.S., Poulter, B., Shi, X.Y., Wang, X.H., Wang, Y.P., Zeng, H., 2016. Global patterns and climate drivers of water-use efficiency in terrestrial ecosystems deduced from satellite-based datasets and carbon cycle models. Glob. Ecol. Biogeogr. 25 (3), 311–323.

Tan, Z.H., Zhang, Y.P., Deng, X.B., Song, Q.H., Liu, W.J., Deng, Y., Tang, J.W., Liao, Z.Y., Zhao, J.F., Song, L., Yang, L.Y., 2015. Interannual and seasonal variability of water use efficiency in a tropical rainforest: results from a 9 year eddy flux time series. J. Geophys. Res.-Atmos. 120 (2), 464–479.

Tao, H., Borth, H., Fraedrich, K., Su, B.D., Zhu, X.H., 2014. Drought and wetness variability in the Tarim River Basin and connection to large-scale atmospheric circulation. Int. J. Climatol. 34 (8), 2678–2684.

Tao, M.H., Chen, L.F., Wang, Z.F., Wang, J., Che, H.Z., Xu, X.G., Wang, W.C., Tao, J.H., Zhu, H., Hou, C., 2017. Evaluation of MODIS deep blue aerosol algorithm in desert region of East Asia: ground validation and intercomparison. J. Geophys. Res.-Atmos. 122 (19), 10329–10340.

Thomey, M.L., Collins, S.L., Vargas, R., Johnson, J.E., Brown, R.F., Natvig, D.O., Friggens, M.T., 2011. Effect of precipitation variability on net primary production and soil respiration in a Chihuahuan Desert grassland. Glob. Chang. Biol. 17 (4), 1505–1515.

Thomson, A.M., Calvin, K.V., Smith, S.J., Kyle, G.P., Volke, A., Patel, P., Delgado-Arias, S., Bond-Lamberty, B., Wise, M.A., Clarke, L.E., Edmonds, J.A., 2011. RCP4.5: a pathway for stabilization of radiative forcing by 2100. Clim. Chang. 109 (1–2), 77–94.

Tian, H.Q., Chen, G.S., Liu, M.L., Zhang, C., Sun, G., Lu, C.Q., Xu, X.F., Ren, W., Pan, S.F., Chappelka, A., 2010. Model estimates of net primary productivity, evapotranspiration, and water use efficiency in the terrestrial ecosystems of the southern United States during 1895-2007. For. Ecol. Manag. 259 (7), 1311–1327.

Tian, H.Q., Lu, C.Q., Chen, G.S., Xu, X.F., Liu, M.L., Ren, W., Tao, B., Sun, G., Pan, S.F., Liu, J.Y., 2011. Climate and land use controls over terrestrial water use efficiency in monsoon Asia. Ecohydrology 4 (2), 322–340.

Tong, X.J., Li, J., Yu, Q., Qin, Z., 2009. Ecosystem water use efficiency in an irrigated cropland in the North China Plain. J. Hydrol. 374 (3–4), 329–337.

Vicente-Serrano, S.M., Begueria, S., Lopez-Moreno, J.I., 2010. A multiscalar drought index sensitive to global warming: the standardized precipitation evapotranspiration index. J. Clim. 23 (7), 1696–1718.

Wang, K.C., Dickinson, R.E., 2012. A review of global terrestrial evapotranspiration: observation, modeling, climatology, and climatic variability. Rev. Geophys. 50 (2), 54.

Wang, X.P., Li, X.R., Xiao, H.L., Berndtsson, R., Pan, Y.X., 2007a. Effects of surface characteristics on infiltration patterns in an arid shrub desert. Hydrol. Process. 21 (1), 72–79.

Wang, X.P., Young, M.H., Yu, Z., Li, X.R., Zhang, Z.S., 2007b. Long-term effects of restoration on soil hydraulic properties in revegetation-stabilized desert ecosystems. Geophys. Res. Lett. 34 (24), 1061–1064.

Wang, H.J., Sun, J.Q., Chen, H.P., Zhu, Y.L., Zhang, Y., Jiang, D.B., Lang, X.M., Fan, K., Yu, E.T., Yang, S., 2012. Extreme climate in China: facts, simulation and projection. Meteorol. Z. 21 (3), 279–304.

Wang, F., Pan, X.B., Wang, D.F., Shen, C.Y., Lu, Q., 2013. Combating desertification in China: past, present and future. Land Use Policy 31, 311–313.

Wang, W., Zhu, Y., Xu, R.G., Liu, J.T., 2015. Drought severity change in China during 1961-2012 indicated by SPI and SPEI. Nat. Hazards 75 (3), 2437–2451.

Warszawski, L., Frieler, K., Huber, V., Piontek, F., Serdeczny, O., Schewe, J., 2014. The inter-sectoral impact model Intercomparison project (ISI-MIP): project framework. Proc. Natl. Acad. Sci. U. S. A. 111 (9), 3228–3232.

Xiao, Z.Q., Liang, S.L., Wang, J.D., Chen, P., Yin, X.J., Zhang, L.Q., Song, J.L., 2014. Use of general regression neural networks for generating the GLASS leaf area index product from time-series MODIS surface reflectance. IEEE Trans. Geosci. Remote Sens. 52 (1), 209–223.

Yang, X.H., He, Q., Mamtimin, A., Huo, W., Liu, X.C., 2013. Diurnal variations of saltation activity at Tazhong: the hinterland of Taklimakan Desert. Meteorog. Atmos. Phys. 119 (3–4), 177–185.

Yao, J.Q., Zhao, Y., Chen, Y.N., Yu, X.J., Zhang, R.B., 2018. Multi-scale assessments of droughts: a case study in Xinjiang, China. Sci. Total Environ. 630, 444–452.

Yu, G.R., Wang, Q.F., Zhuang, J., 2004. Modeling the water use efficiency of soybean and maize plants under environmental stresses: application of a synthetic model of photosynthesis-transpiration based on stomatal behavior. J. Plant Physiol. 161 (3), 303–318.

Yu, G.R., Wen, X.F., Sun, X.M., Tanner, B.D., Lee, X.H., Chen, J.Y., 2006. Overview of ChinaFLUX and evaluation of its eddy covariance measurement. Agric. For. Meteorol. 137 (3–4), 125–137.

Yu, G.R., Song, X., Wang, Q.F., Liu, Y.F., Guan, D.X., Yan, J.H., Sun, X.M., Zhang, L.M., Wen, X.F., 2008. Water-use efficiency of forest ecosystems in eastern China and its relations to climatic variables. New Phytol. 177 (4), 927–937.

Yu, Z., Wang, J.X., Liu, S.R., Rentch, J.S., Sun, P.S., Lu, C.Q., 2017. Global gross primary productivity and water use efficiency changes under drought stress. Environ. Res. Lett. 12 (1), 10.

Zhang, Z.H., Huisingh, D., 2018. Combating desertification in China: monitoring, control, management and revegetation. J. Clean. Prod. 182, 765–775.

Zhang, Y., Zhang, X.L., 2017. Estimation of net primary productivity of different forest types based on improved CASA model in Jing-Jin-Ji region, China. J. Sustain. For. 36 (6), 568–582.

Zhang, Z., Jiang, H., Liu, J.X., Han, J.J., Zhu, Q.A., Zhang, X.Y., 2013. Implications of future water use efficiency for ecohydrological responses to climate change and spatial heterogeneity of atmospheric CO_2 in China. Terr. Atmos. Ocean. Sci. 24 (3), 451–465.

Zhang, F.M., Ju, W.M., Shen, S.H., Wang, S.Q., Yu, G.R., Han, S.J., 2014. How recent climate change influences water use efficiency in East Asia. Theor. Appl. Climatol. 116 (1–2), 359–370.

Zhang, T., Peng, J., Liang, W., Yang, Y.T., Liu, Y.X., 2016. Spatial-temporal patterns of water use efficiency and climate controls in China's Loess Plateau during 2000-2010. Sci. Total Environ. 565, 105–122.

Zhang, C.L., Shen, Y.P., Li, Q., Jia, W.R., Li, J., Wang, X.S., 2018. Sediment grain-size characteristics and relevant correlations to the aeolian environment in China's eastern desert region. Sci. Total Environ. 627, 586–599.

Zhao, C., Wang, Y., Hu, S., Li, Y., 2004. Effects of spatial variability on estimation of evapotranspiration in the continental river basin. J. Arid Environ. 56 (2), 373–382.

Zhao, H.L., Guo, Y.R., Zhou, R.L., Drake, S., 2011. The effects of plantation development on biological soil crust and topsoil properties in a desert in northern China. Geoderma 160 (3–4), 367–372.

Zheng, H., Yu, G.R., Wang, Q.F., Zhu, X.J., Yan, J.H., Wang, H.M., Shi, P.L., Zhao, F.H., Li, Y.N., Zhao, L., Zhang, J.H., Wang, Y.F., 2017. Assessing the ability of potential evapotranspiration models in capturing dynamics of evaporative demand across various biomes and climatic regimes with ChinaFLUX measurements. J. Hydrol. 551, 70–80.

Zhou, Q.L., Jiang, D.M., Liu, Z.M., Alamusa, Li, X.H., 2013. Effect of leaching on loss of soil phosphorus in different types of sand dune in Horqin Sandy Land, China. In: Zhao, J., Iranpour, R., Li, X., Jin, B. (Eds.), Advances in Environmental Technologies, Pts 1–6. Advanced Materials Research. Trans Tech Publications Ltd, Stafa-Zurich, pp. 3818–3827.

Zhu, W.Q., Pan, Y.Z., Liu, X., Wang, A.L., 2006. Spatio-temporal distribution of net primary productivity along the Northeast China Transect and its response to climatic change. J. For. Res. 17 (2), 93–98.

Zhu, X.J., Yu, G.R., Wang, Q.F., Hu, Z.M., Zheng, H., Li, S.G., Sun, X.M., Zhang, Y.P., Yan, J.H., Wang, H.M., Zhao, F.H., Zhang, J.H., Shi, P.L., Li, Y.N., Zhao, L., Zhang, F.W., Hao, Y.B., 2015. Spatial variability of water use efficiency in China's terrestrial ecosystems. Glob. Planet. Chang. 129, 37–44.